The Chironico landslide (Valle Leventina, southern Swiss Alps): age and evolution

Anne Claude · Susan Ivy-Ochs · Florian Kober · Marco Antognini ·
Bernhard Salcher · Peter W. Kubik

Abstract In this study, we focus on the postglacial Chironico landslide in Valle Leventina, the valley of the Ticino river immediately south of the Gotthard pass (southern Swiss Alps). At Chironico, 530 million m^3 of granite gneiss detached from the eastern wall of Valle Leventina and slid along valley-ward dipping foliation joints and fractures. The slide mass was deposited into the valley bottom and blocked the Ticino river, as well as a tributary, the Ticinetto stream, on the opposite side of the valley. Wood fragments found in lacustrine sediments in the slide-dammed upstream lake were previously dated, yielding a minimum age for the landslide of approximately 13,500 cal years BP. Based on the deposit morphology, the landslide was in the past interpreted as being composed of two events. In order to directly date the landslide, ten boulders were dated using the cosmogenic nuclides [10]Be and [36]Cl. Mean exposure ages indicate that the landslide occurred at 13.38 ± 1.03 ka BP, during the Bølling-Allerød interstadial. This implies that the Chironico landslide, one of the few pre-Holocene slides known in Alps, is also the oldest in crystalline rock. With runout modelling using DAN3D we could reproduce the hypothesized single-event failure scenario, as well as the character and extent of motion of the landslide mass. Both the ages and the modelling suggest that the landslide was released in one event around 3,000 years following deglaciation.

Keywords Switzerland · Canton ticino · Surface exposure dating · Cosmogenic nuclides ([10]Be, [36]Cl) · Landslide modelling

A. Claude · F. Kober · B. Salcher
Geological Institute, ETH Zurich, Sonneggstrasse 5,
8092 Zurich, Switzerland

S. Ivy-Ochs · P. W. Kubik
Laboratory of Ion Beam Physics (LIP), ETH Zurich,
Otto-Stern-Weg 5, 8093 Zurich, Switzerland

S. Ivy-Ochs
Department of Geography, University of Zurich,
Winterthurerstrasse 190, 8057 Zurich, Switzerland

M. Antognini
Museo Cantonale di storia naturale, Viale Cattaneo 4,
6900 Lugano, Switzerland

A. Claude (✉)
Institute of Geological Sciences, University of Bern,
Baltzerstrasse 1-3, 3012 Bern, Switzerland
e-mail: anne.claude@geo.unibe.ch

Present Address:
F. Kober
Nagra, Hardstrasse 73, Postfach 280, 5430 Wettingen,
Switzerland

Present Address:
B. Salcher
Department of Geography and Geology, Salzburg University,
Hellbrunner Strasse 34, 5020 Salzburg, Austria

1 Introduction

The interaction of rock uplift with surface processes results in the development of mountain topography. As a major mechanism for bedrock erosion, landslides control the

variability of sediment flux from tectonically active mountain ranges (Hovius et al. 1997; Shroder and Bishop 1998) and have therefore a long term impact on landscape evolution in mountain chains (Hovius and Stark 2007). Mass wasting sets geomorphic control on fluvial processes (Hovius and Stark 2007; Korup et al. 2010) since hillslopes have to adjust to changes in fluvial incision rates in response to rock uplift. It is suggested that mass wasting processes (landslides, debris flows) in valleys with critical slopes or relief (Korup et al. 2010) are influenced by climate and that they thus may be regarded as a geomorphological proxy for climate change (Borgatti and Soldati 2010 and references therein). Preparatory factors for landslides in contrast to triggering factors need to accumulate over a long time period in order to induce failure (Gunzburger et al. 2005). Some of these preparatory conditions include gradual rock weathering, frost action, changes in pore water pressure and stress redistribution during or after glacial unloading (e.g. Gunzburger et al. 2005; Prager et al. 2008; Korup et al. 2010). Important triggering factors are heavy rainfall or earthquakes, which have as a consequence a direct collapse of the slope, as shown by more recent events in Alpine realm (Fritsche and Fäh 2009).

The retreat of the late Pleistocene glaciers has played an important part in preconditioning numerous landslides in mountain valleys (Ballantyne et al. 2014a). By applying various dating techniques it has been demonstrated for the Central Alps that the majority of dated landslides were not released immediately after the end of the last glaciation but a few thousand years later, during the Lateglacial and Holocene (Heuberger 1994; Ivy-Ochs et al. 1998, 2009; Poschinger 2002; Gruner 2006; Prager et al. 2007, 2008). In the Alps, some of the largest landslides cluster in the early Holocene around 10,500–9,400 cal years BP (Soldati et al. 2004; Prager et al. 2008). A marked period of increased landslide activity was also assigned to the Subboreal in the middle Holocene, from 4,200 to 3,000 cal years BP (Dapples et al. 2003; Prager et al. 2007), accompanying climatic deterioration with a shift towards colder and more humid conditions. Raetzo-Brühlhart (1997), Dapples et al. (2003), Soldati et al. (2004), Gruner (2006) and Prager et al. (2008) discuss several intervals of enhanced slope instability during the late Holocene in the Swiss Alps (6,250–4,800; 3,500–2,100; 1,700–1,150; 750–300 cal years BP), Austrian Alps (4,200–3,000 cal years BP), and also in the Italian Alps (5,800–2,000 cal years BP).

The Chironico landslide in the Valle Leventina of the southern Swiss Alps (canton Ticino) (Fig. 1), with an estimated volume of 530 million m^3, is among one of the largest landslides in the Alps in crystalline rock, after the Köfels landslide in the Austrian Ötztal (Abele 1974). The accumulation area of the landslide is subdivided into two different lobes (Fig. 2), which are separated by the Ticinetto river, a tributary of the Ticino river. Earlier work by Naegeli (1920) and Dal Vesco (1979) suggested that the Chironico landslide consisted of two events because of the apparent dual-lobe morphology of the deposit and the mapping of two separate detachment scarps. Dal Vesco (1979) moreover argued that the boulders of the southern deposit have a morphology distinguishable from those of the northern deposit, having somewhat smaller size.

Antognini and Volpers (2002) investigated the Chironico landslide by looking at cores taken for geotechnical purposes. They radiocarbon dated pieces of wood found in lacustrine sediments of the landslide-dammed lake, located north of the deposit (location S5 in Fig. 2). The wood fragments yielded a minimum age of approximately 13,500 cal years BP (Antognini and Volpers 2002). Since they originate from a secondary deposit and were not found at the base of the core, and furthermore because wood can easily be washed in by flood events, questions remained about the absolute age of the Chironico landslide event itself. In addition, no information was gained on the question of whether the event consisted of one or two slides. In this work, we date the Chironico landslide deposit directly using surface exposure dating with the cosmogenic nuclides ^{10}Be and ^{36}Cl. The goals of this study are to reconstruct not only the event chronology and subsequent landscape evolution of the Chironico area (Fig. 2), but also to explore the dynamics of the landslide. Furthermore, we aim to evaluate the long-standing debate about this landslide, namely if it resulted from one single event or even several successive slides (Naegeli 1920; Dal Vesco 1979; Antognini and Volpers 2002), and to further constrain the release area, as the detachment scarp on the eastern valley wall is difficult to locate.

2 Geologic and geomorphologic setting

The Chironico area is dominated by bedrock of the Lower Penninic Simano- and Leventina nappes (Antognini and Volpers 2002). The Simano nappe is composed of several orthogneiss bodies intruded into paragneisses and schists (Ruetti et al. 2005), whereas the Leventina nappe consists of mainly orthogneisses (Fig. 3), including the so-called "Leventina Granitic Gneiss" (Casasopra 1939), that often shows an augen-gneiss texture (Timar-Geng et al. 2004). In a few locations, Triassic quartzites separate the Simano nappe from the underlying Leventina nappe (Niggli et al. 1936). In all rock types, a well-developed foliation occurs which dips towards SSW at angles ranging from 25° to 30°, generating a dip-slope on the eastern valley flank (Antognini and Volpers 2002).
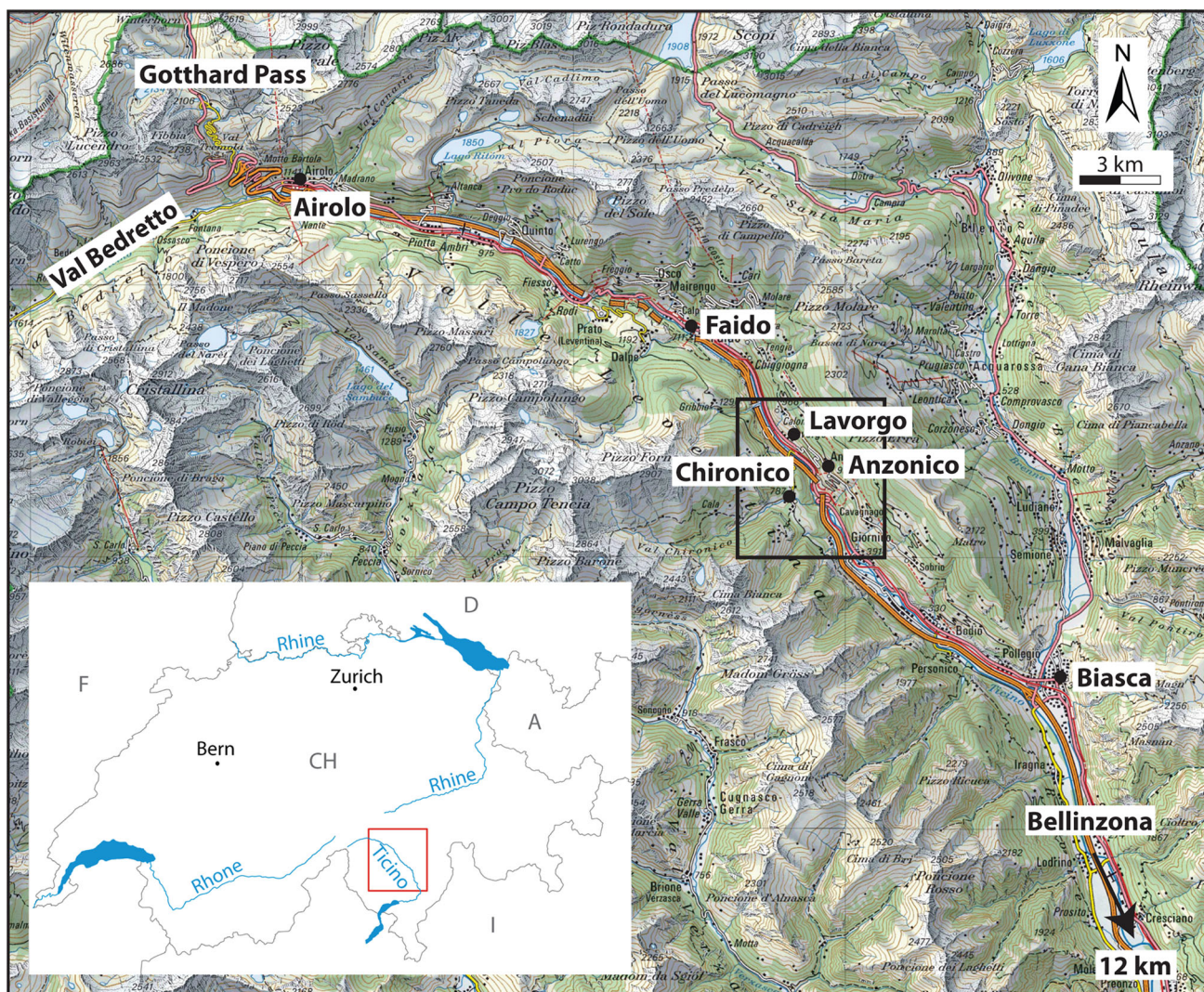
Fig. 1 Topographic overview map of the study area (© Federal Office of Topography, swisstopo, CH-3084 Wabern). Valle Leventina is situated between Airolo and Biasca. The *black square* locates the digital elevation model (DEM) of the Chironico landslide as can be seen in Fig. 2

During the Last Glacial Maximum (LGM), the Valle Leventina was almost entirely filled with ice except for nunataks, represented by the mountain peaks to the east and west of the valley (Bini et al. 2009). Clear evidence which can be used to unravel the sequence of events during deglaciation of the Valle Leventina is rare. This is partly because of the lack of lateral moraines due to the steep valley flanks (Hantke 1983), as well as the possibility that any end moraines may be buried under the large amount of alluvial fill (as suggested elsewhere; Ivy-Ochs et al. 2006). Renner (1982) mapped moraines and assigned glacial stadials in the Val Bedretto (west of Airolo, Fig. 1). He suggested that the Airolo stadial represents the Gschnitz stadial as defined in the Eastern Alps (Gross et al. 1978; Maisch 1981) based on similar equilibrium line altitude (ELA) depressions. Renner did not report any younger

stadials reaching into the Valle Leventina. Hantke (1983) mapped different ice margins in the Leventina near Biasca and Bellinzona (Fig. 1), which he classified as older than the Gschnitz stadial (16–17 ka BP; Ivy-Ochs et al. 2006). These observations imply that following the Gschnitz stadial, the Valle Leventina was ice free.

3 Methods

3.1 Field investigations and reconstruction of pre-failure valley topography

The extent of the Chironico landslide was investigated and mapped in the field with the aid of 2-m resolution bare-earth LiDAR data provided by *Ufficio della misurazione*
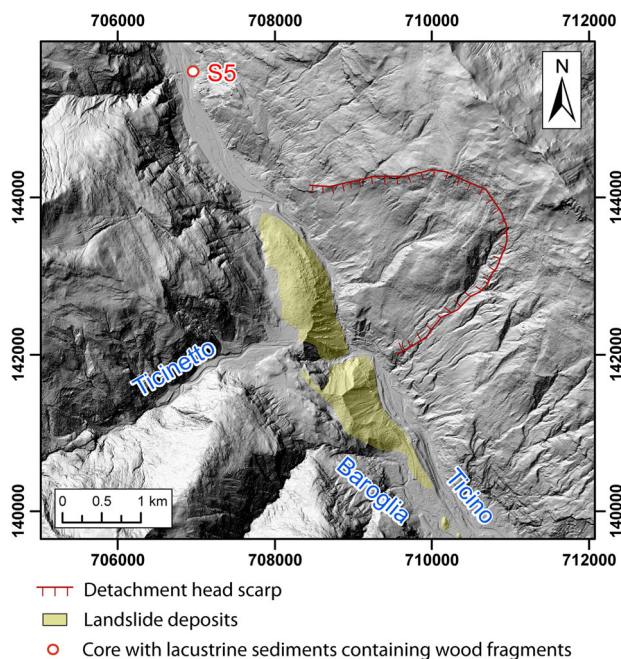
Fig. 2 Hillshade of the digital elevation model (DEM, 2 m resolution) of the Chironico landslide (for location see Fig. 1). The Chironico landslide is seen in the *centre*, forming a blockage of the river valley, whereas the detachment scarp is located on the eastern valley flank. S5 shows the location of the borehole in which the wood pieces were found in lacustrine sediments. DEM model reproduced with the authorization of the *Ufficio della misurazione ufficiale e della geoinformazione (UMG)* of the canton of Ticino, dated 1.7.2011. Coordinates of the Swiss national grid CH1903 (LV03)

ufficiale e della geoinformazione (UMG: land surveying and geo-information office, canton Ticino). Mapping focused on bedrock and landslide deposits and their contacts. In addition, all surrounding Quaternary depositional and erosional landscape elements in the area were mapped. The surface morphology of the landslide and distribution of boulder size was documented. To facilitate the characterization of the two landslide lobes and the visualization of the incision by the rivers, a slope map was created in ArcGIS (Fig. 4).

In order to calculate the volume of the Chironico landslide and to construct a runout model, the pre-failure Valle Leventina was reconstructed. The glacial valley trough topography and the glacial valley slope topography were reconstructed in two steps: Firstly, the delineation of the pre-failure trough topography was based on borehole information from drillings within the Valle Leventina (unpublished reports GESPOS Database (*Gestione Sondaggi, Pozzi e Sorgenti:* Drilling, boreholes and springs database); SUPSI, Trevano, Ticino (*Scuola Universitaria e Professionale della Svizzera Italiana,* Instituto Scienze della Terra: University of Applied Sciences and Arts of Southern Switzerland, Institute of Earth Sciences). In total,

250 cores are documented in the database, of which 40 located in the study area were used for further investigations. Derived point data were then interpolated to a surface together with contour information of the modern valley topography (outside the pre-failure area). Secondly, the pre-failure topography at the position of the postulated landslide sliding surface (glacial valley slope) was reconstructed by creating a simplified geometry of a typical glacial trough showing one clear break in slope as observed in the main valley (see also Ambrosi and Crosta 2011). The approximate volume of the Chironico landslide was then calculated by subtracting the pre-failure model from the current topography of the Valle Leventina. However, this resulted only in a minimum value for the volume of the landslide. The post-slide erosion of the deposit had to be taken into account and was added to the previously calculated volume.

3.2 Runout modelling

In order to validate potential failure scenarios and investigate the character and extent of landslide motion (Hungr and McDougall 2009), we performed a runout modelling exercise using a program for the analysis of rapid 3D mass movements (DAN3D; McDougall and Hungr 2004). The model is based on volume estimates of the landslide and uses as input topography files (path topography file and a source topography file) and rheology-specific material properties (McDougall and Hungr 2004). The path topography file represents the topography of the sliding surface and was created by removing the material in the release area and accumulation area in the valley. The source topography file defines the vertical depth of the sliding mass before its release. This file was generated by subtracting the current valley topography from the pre-failure topography in the release area and taking into account a bulking factor of 30 %. Furthermore, the model allows different rheologies (e.g. frictional or Voellmy) to represent the basal sliding surface (Hungr and Evans 1996). Rheological parameters were adjusted in such a way that they reproduced the runout distance and also the lateral expansion of the landslide (Sosio et al. 2011). Assuming a frictional rheology, values for the basal friction angle used by other investigators vary between 11° and 31° (e.g. Hungr and Evans 1996; Sosio et al. 2011). For the internal friction angle, typical values range between 30° and 40° (e.g. McDougall and Hungr 2004; Pirulli et al. 2007; Sosio et al. 2008).

3.3 Surface exposure dating

The cosmogenic nuclide surface exposure dating method is based on the concept that cosmogenic nuclides (e.g. ^{10}Be,

Fig. 3 Geological and geomorphological map of the Chironico landslide and the surrounding parts of Valle Leventina based on 'Geologische Karte der Tessineralpen 1:50,000' (Preiswerk et al. 1934), Naegeli (1920), and our own mapping and GIS interpretation
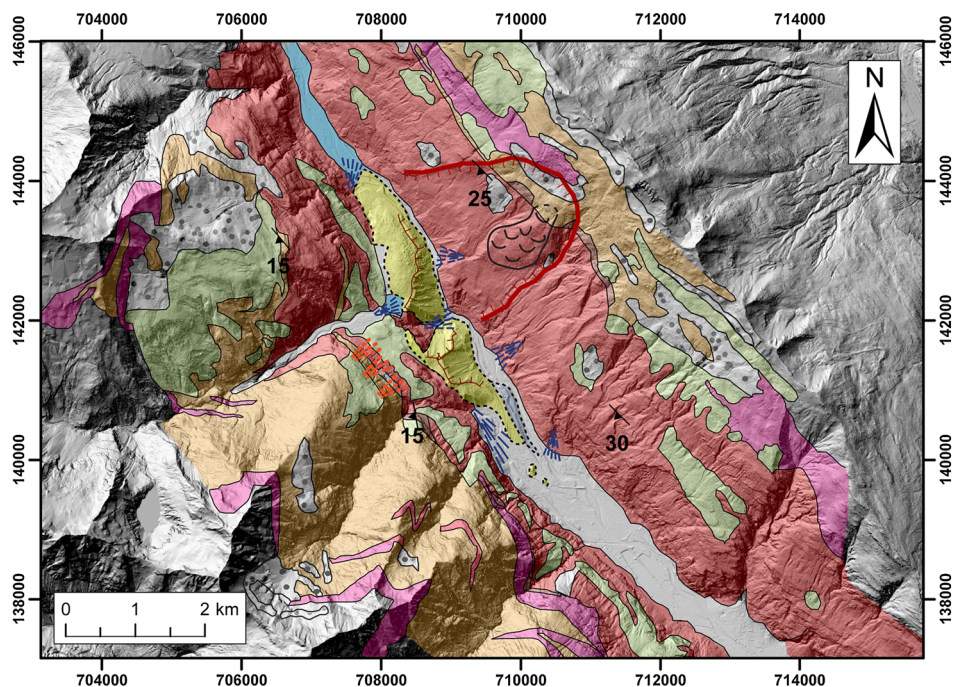
Legend

| Dip of foliation |
| Detachment head scarp |
| Erosion scarp |
| Contact certain |
| Contact uncertain/inferred |

Quaternary landforms

- Landslide deposits
- Paleolake (inferred extent)
- Fluvial terraces
- Alluvium
- Alluvial fan
- Talus, cones
- Sackung
- Glacial and glaciofluvial sediments (LGM, Lateglacial)

Bedrock

- Quartzite
- Biotite Gneiss and Micaschists (Paragneiss; Simano nappe)
- Orthogneiss of the Simano nappe
- Granite Gneiss (Leventina Gneiss, Orthogneiss; Leventina nappe)

^{36}Cl) build-up with time in minerals exposed to cosmic rays (e.g. Lal 1991; Gosse and Philips 2001). The radionuclide ^{10}Be is produced by several reactions; the most common one is spallation (Gosse and Philips 2001). During this reaction, secondary cosmic ray particles hit the surface of the target element and one or more lighter particles are ejected from the nucleus, leaving the cosmogenic nuclide in the mineral lattice (Gosse and Philips 2001). In the case of the radionuclide ^{36}Cl, several reactions are involved: spallation of ^{40}Ca and ^{39}K, muon-induced reactions on ^{40}Ca and ^{39}K and low energy neutron capture by ^{35}Cl and ^{39}K (Gosse and Philips 2001; Alfimov and Ivy-Ochs 2009).

3.3.1 Sampling

In total twelve boulders were sampled by taking approximately several hundred grams of material from the upper few centimetres of boulders on the surface of the landslide deposits, using hammer and chisel. Boulders that are strongly shielded by surrounding hillslopes or neighbouring boulders were avoided (Ivy-Ochs and Kober 2008). All boulders were measured for topographic shielding by surrounding mountains using a clinometer. The selected boulders did not show any obvious signs of damage or spalling. To address the question that there might have been two successive landslides, samples from both lobes of the landslide accumulation area were taken (Fig. 5). From the twelve samples, three did not have enough pure quartz after the leaching to continue. Chi-2b is the only sample where some material was left after leaching; this is therefore the only sample which could be dated using ^{36}Cl.

3.3.2 Sample preparation

The collected rocks were crushed and sieved to obtain a grain size range <0.5 mm, followed by chemical

Fig. 4 Slope-map showing the steepness of the Chironico landslide and adjacent hillslopes. *Red areas* indicate a high slope whereas green areas have a lower slope. *The dashed line* shows the landslide depositional lobes whereas the hachured *solid line* represents the detachment head scarp. The direction of the view for Fig. 5 is shown by the *black square*
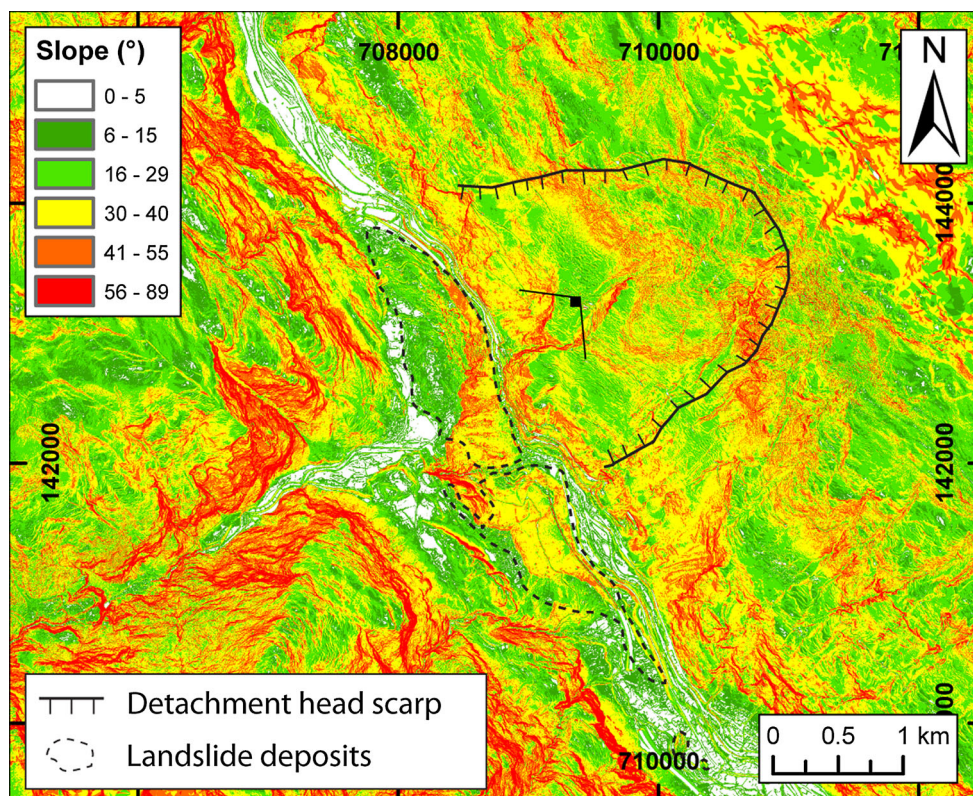

Fig. 5 Photograph panorama of the Chironico landslide deposits, with the sampling sites, looking SW from viewpoint indicated on Fig. 4

preparation according to Ivy-Ochs (1996), Ochs and Ivy-Ochs (1997) and von Blanckenburg et al. (1996). The pre-treatment involved several leaching steps of approximately 100 g of crushed rock in dilute HF to ensure a pure quartz fraction and also to erase any possible meteoric ^{10}Be contamination. 0.250 mg of carrier ^{9}Be was added to approximately 30 g of leached quartz, which then was dissolved using concentrated HF and HNO$_3$. In a first step, the samples were run through anion exchange columns to remove iron and were precipitated as hydroxides. In a

second step, Be was extracted by running the samples dissolved with oxalic acid through a cation exchange column. Be(OH)$_2$ was then precipitated at pH 8 with NH$_4$OH and transferred to quartz crucibles, followed by baking in a furnace at 675 °C (Fe–Ag method for the Tandem accelerator; Akçar et al. 2012) or 850 °C for measurements on the Tandy accelerator.

Sample preparation for ^{36}Cl dating is described in detail by Ivy-Ochs (1996) and Ivy-Ochs et al. (2004). About 100 g of sample was leached with weak HNO$_3$, followed

by rinsing with water in order to remove any possible meteoric Cl. The leached sample was dissolved with 2.4 mg of carrier ^{35}Cl using HNO_3. A solution of $AgNO_3$ was added to precipitate AgCl. As ^{36}S is an interfering isobar in ^{36}Cl accelerator mass spectrometry (AMS), $Ba(NO_3)_2$ was added to remove sulfur (Ivy-Ochs et al. 2009).

3.3.3 AMS measurement and age calculation

^{10}Be was measured at the AMS facility in the Laboratory of Ion Beam Physics at ETH Zurich, Switzerland, using both the 0.5 MV Tandy (Müller et al. 2010) and 6 MV Tandem accelerator (Table 1, samples with a). The ^{10}Be/^{9}Be ratios for both accelerators (Kubik and Christl 2010; Müller et al. 2010) were measured against ETH in-house standards calibrated to 07KNSTD standard of Nishiizumi et al. (2007). All ratios were corrected for a blank value of $3.0 \pm 0.5 \times 10^{-15}$, which is consistent for both machines. The ^{10}Be surface exposure ages were then calculated using the Northeastern North America production rate of the CRONUS-Earth online calculator (Balco et al. 2008, 2009), assuming a ^{10}Be half-life of 1.39 ± 0.012 Ma (Chmeleff et al. 2010; Korschinek et al. 2010). Scaling for geographic latitude and altitude was made according to the time-dependent model of Lal (1991) and Stone (2000) assuming a spallation production rate of $PR_{SP} = 3.88 \pm 0.19$ ^{10}Be atoms g^{-1} a^{-1}. The

shielding correction was carried out using the geometric shielding calculator of the CRONUS-Earth online calculator.

At the ETH Zurich AMS facility (Synal et al. 1997), total Cl and ^{36}Cl were determined using the method of isotope dilution (Ivy-Ochs et al. 2004; Desilets et al. 2006). The ^{36}Cl/Cl value is measured against the ETH internal standard K381/4N with a value of ^{36}Cl/Cl $= 17.36 \times 10^{-12}$ and the ratio was corrected for a blank value of 2.3×10^{-15}. Major element concentrations, determined by ICP-MS at SGS (Ontario, Canada), were used to calculate the production rates and the amount of neutrons available for the neutron capture pathway for production of ^{36}Cl (Alfimov and Ivy-Ochs 2009). The ^{36}Cl exposure age was calculated using an in-house age calculator (following Alfimov and Ivy-Ochs 2009), using the production rates of 48.8 ± 3.4 ^{36}Cl atoms (g Ca)$^{-1}$ year^{-1} (Stone et al. 1996) and 5.2 ± 1.0 ^{36}Cl atoms (g Ca)$^{-1}$ year^{-1} (Stone et al. 1998) for spallation and muon capture on Ca, respectively, and 161 ± 9 and 10.2 ± 1.3 ^{36}Cl atoms (g K)$^{-1}$ year^{-1} (Evans et al. 1997) for spallation and muon capture on K. Production of ^{36}Cl through neutron capture followed the procedures of Liu et al. (1994) and Phillips et al. (2001) using a value of 760 ± 150 neutrons g_air^{-1} year^{-1} (Alfimov and Ivy-Ochs 2009). We used a surface erosion rate of 1 mm ka^{-1} for calculation with both nuclides, as the surface structures of the boulders show no deep weathering.

Table 1 AMS measured concentrations of ^{10}Be and calculated surface exposure ages for the Chironico landslide

Sample name	Latitude (DD.DD)	Longitude (DD.DD)	Elevation (m)	Boulder height (m)	Sample thickness (cm)	Quartz dissolved (g)	Shielding correction factor	^{10}Be (at/g) $\times 10^3$	Error (at/g) $\times 10^3$	Exposure age (ka)	Erosion corrected ages using 1 mm ka^{-1} (ka)
Chi-1	46.4155	8.8524	761	3.0	2.0	32.2443	0.9773	104.00	5.38	13.92 ± 0.72 (0.99)	14.09 ± 0.74 (1.01)
Chi-3	46.4139	8.8543	742	2.0	5.0	10.8599	0.9818	97.71	7.64	13.57 ± 1.06 (1.25)	13.72 ± 1.09 (1.28)
Chi-4	46.4161	8.8516	764	1.5	3.0	30.3292	0.9500	94.92	5.08	13.14 ± 0.71 (0.95)	13.29 ± 0.72 (0.97)
Chi-5a-2[a]	46.4280	8.8488	815	15.0	5.0	29.6500	0.9500	99.83	7.29	13.47 ± 0.99 (1.19)	13.62 ± 1.01 (1.21)
Chi-6	46.4271	8.8493	802	6.0	2.0	31.7128	0.9500	96.54	5.34	12.84 ± 0.71 (0.95)	12.98 ± 0.73 (0.97)
Chi-7	46.4271	8.8490	805	3.0	2.5	29.6054	0.9794	98.93	5.34	12.80 ± 0.69 (0.93)	12.94 ± 0.71 (0.95)
Chi-10[a]	46.4186	8.8490	801	3.0	2.0	31.6899	0.9772	82.17	5.93	10.63 ± 0.77 (0.93)	10.73 ± 0.79 (0.94)
Chi-11[a]	46.4174	8.8502	800	2.0	1.0	24.7579	0.9772	118.85	7.96	15.27 ± 1.03 (1.27)	15.46 ± 1.06 (1.30)
Chi-12[a]	46.4238	8.8495	790	5.0	3.0	31.3620	0.9836	99.91	6.79	13.09 ± 0.89 (1.10)	13.23 ± 0.91 (1.12)

[a] Samples were measured on the 6 MV Tandem accelerator, whereas the others were measured on the 0.5 MV Tandy accelerator

4 Results

4.1 Field investigations and reconstruction of pre-failure valley topography

4.1.1 Geomorphology of the Chironico landslide

The Chironico landslide comprises a deposition area on the western side of the Valle Leventina, extending over a length of about 5,300 m (Fig. 3) together with a release area located on the opposite eastern valley flank. From field studies, the landslide release area is not clearly evident due to dense forest cover, and there is no clear expression of a scarp (Schardt 1910; Naegeli 1920; dal Vesco 1979; Antognini and Volpers 2002). LiDAR data and earlier mapping by other authors suggest the scarp shown in Fig. 3. On the LiDAR, smoothness changes can be observed in this area. The topmost part of the scarp shows a rougher surface compared to the surroundings. In addition, the head scarp has been affected by gravitational post-failure deformations, and small-scale recent sliding is observed in the detachment area ('Sackung' in Fig. 3). Antognini and Volpers (2002) also place the scarp here as there is a fairly convex shape in the valley flank.

On the western valley flank, toward the northwest, the landslide deposit shows a contact with Leventina Gneiss bedrock (Fig. 3). However, this contact is not well exposed. The morphology suggests this contact was exploited by streams in the past. Located to the west of the landslide are glacial and glaciofluvial deposits (Fig. 3). No signs of modification of the landslide deposits by ice could be observed in the field. We could locate no glacial deposits on top of the landslide deposits; no erratic boulders, no rounded or striated clasts. Additionally, it is assumed that the surface of the deposit would have been significantly modified if ice had overridden the landslide (Gruber et al. 2009). The images in Fig. 6a–c illustrate the nature of the top surface of the deposit. The original depositional shape and post-depositional incision are shown well on the slope map in Fig. 4. The original
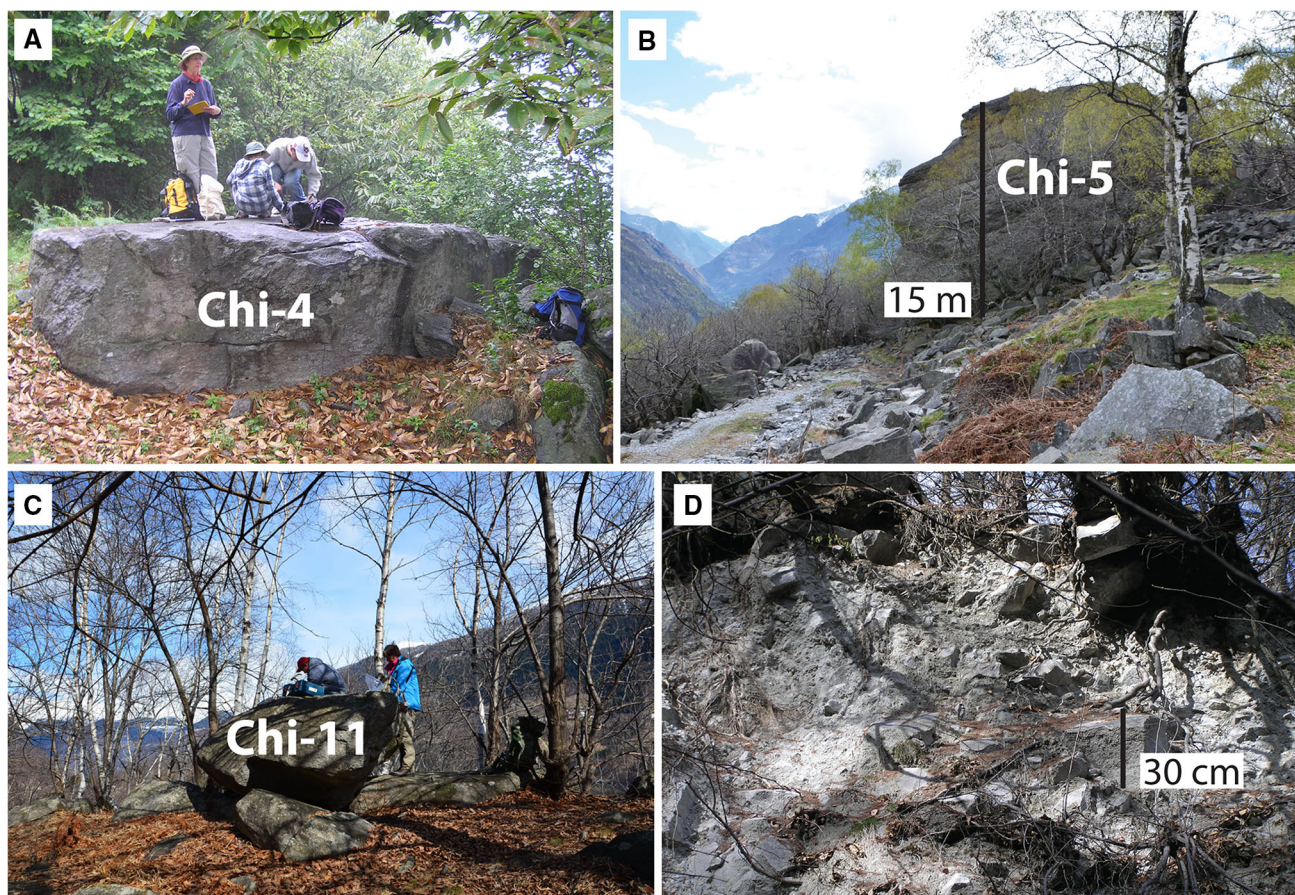

Fig. 6 Photographs of sampled boulders in the landslide accumulation area (photos **a–c**) and a photo showing the internal structure of the landslide deposits (photo **d**). **a** Chi-4 (708620/141588) is located on the southern depositional lobe. **b** Chi-5 (708382/142890) is one of the biggest boulders with a height of around 15 m and belongs to the northern lobe. **c** Chi-11 (708523/141716) is from the southern lobe. **d** Outcrop showing the internal structure of the landslide deposits (708328/142149)

depositional surface can clearly be distinguished from areas incised by the rivers Ticino and Ticinetto. The upper surface of the landslide exhibits a N–S trending broad wall at an elevation between 780 and 820 m, which may be a compressional feature related to the impact of the slide mass against the western valley wall. The landslide deposit does not everywhere show the same slope towards the bottom of the Valle Leventina. In Fig. 4 it is remarkable that the slope of the northern depositional lobe is slightly steeper towards the Ticino. The southern lobe, however, is less steep. The shape and eastern slope of the northern lobe provide crucial information on the shape of the deposit areas before river incision.

Cross sections (Figs. 7, 8) were drawn across the two deposit lobes. The cross-profile of the northern lobe reveals a convex shape of the landslide deposit on the western side with a confined valley bottom (Fig. 8). In contrast, the profile across the southern lobe has a more concave slope with a wider valley bottom (Fig. 8), which is partially alluviated, as can be observed in the slope map (Fig. 4). These observations correlate with the angles of both slopes (Fig. 4) where the steeper northern slope shows that the river incision is still active.

The internal structure of the landslide deposit is illustrated in Fig. 6d and consists of chaotic, monolithological, angular blocks embedded in a fine, unsorted matrix of crushed rock. The angular blocks show sizes ranging from gravel to boulders and the matrix of crushed rock consists of silt, sand and gravel. Various degrees of rock fragmentation can be observed. The crushed rock is rather cohesive as it holds up the steep incised slope in the northern lobe and in the incised valley of the Ticinetto.

In addition to the main landslide deposit, two cone-shaped toma hills (Fig. 3) with heights of 16 and 10 m, respectively, are situated at the southeastern end of the landslide deposit. The toma are located about 400–700 m downstream of the main deposit. It is not certain that these are connected to the principal landslide accumulation since
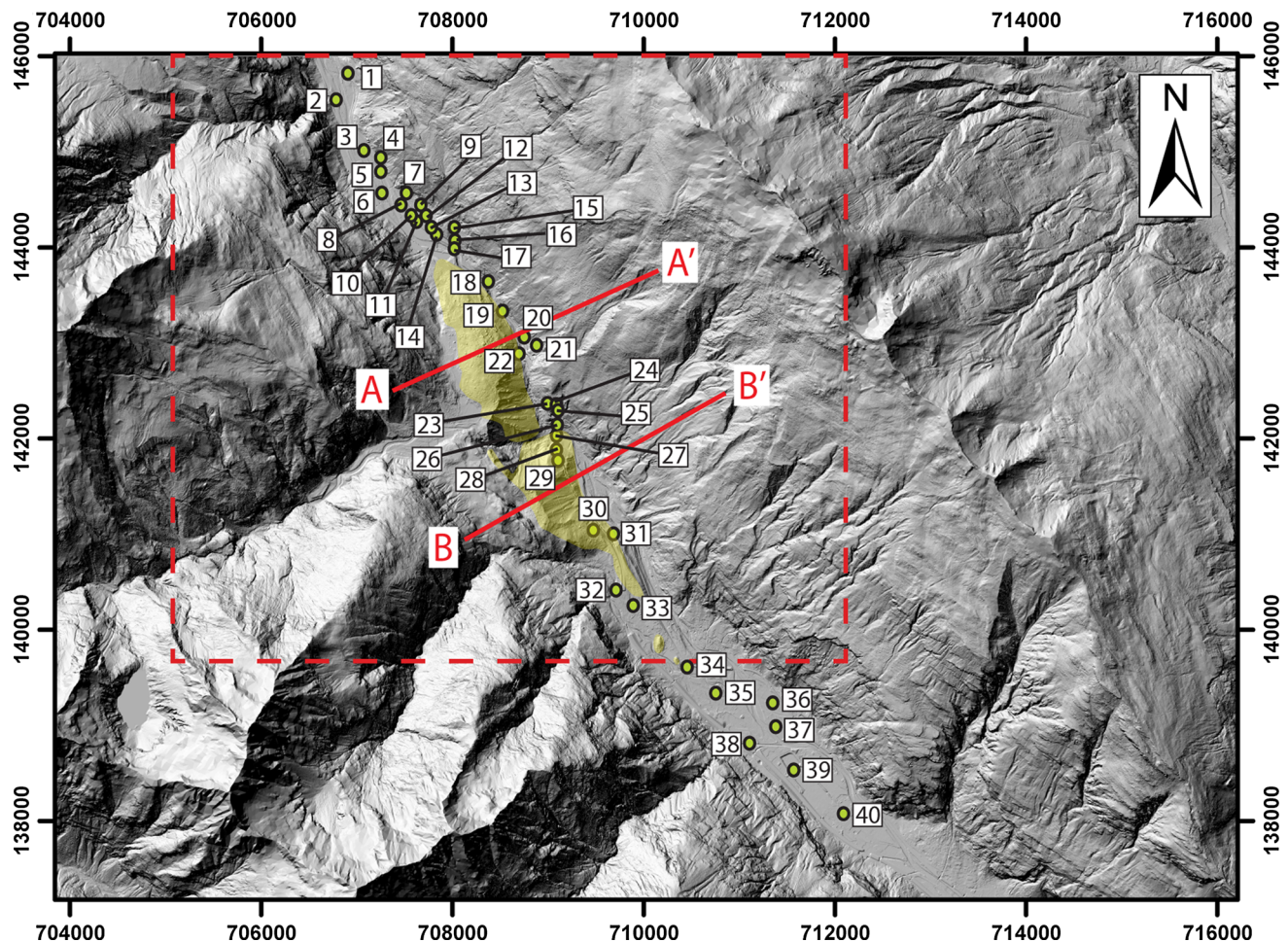

Fig. 7 Locations of the cores within the study area in the Valle Leventina (the coordinates of the sites and the original core names are listed in Online Resource 1). The red profiles A–A′ and B–B′ are cross sections through both depositional lobes (see Fig. 8). The red dashed square marks the outline of Fig. 2
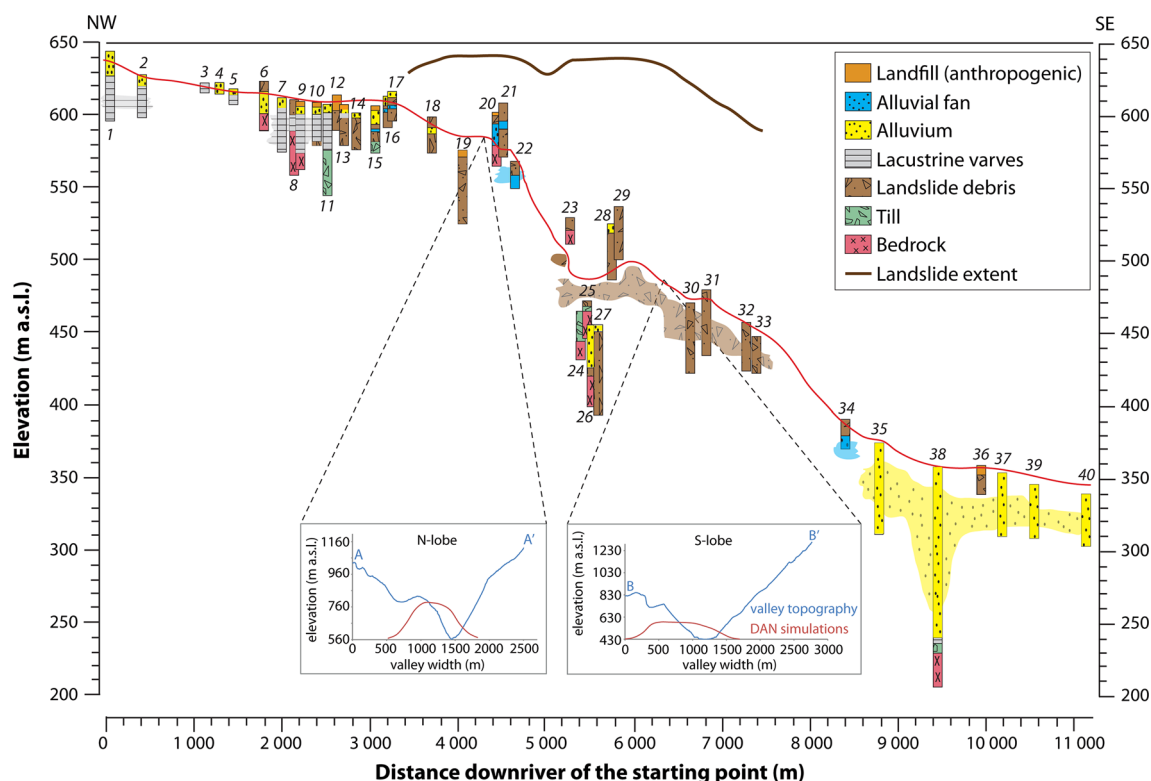
Fig. 8 Synthesis of subsurface data in the vicinity of the Chironico landslide, shown on a profile along the bottom of Valle Leventina, from northwest to southeast. Note that not all the cores are located exactly on the line of profile, thus several were projected into the profile plane. The *red line* represents the topography of the valley bottom; the *thick brown* line is a projection of the upper surface of the landslide into the profile plane. Vertical exaggeration is 15×. A–A′ and B–B′ are cross sections through the northern and southern depositional lobes of the landslide (for location, see Fig. 7). On the cross sections, the blue line is present valley topography whereas the *red line* is modelled landslide topography

there are no drill cores from this location. In other examples of landslides, such deposits are often not connected in the subsurface to the main deposit body (e.g. Abele 1974; Prager et al. 2009).

4.1.2 Pre-failure topography

We reconstructed the pre-failure valley topography in order to understand the evolution of the Valle Leventina around the area of Chironico and as input for the runout model.

4.1.2.1 Subsurface data illustration The stratigraphic log descriptions (Fig. 8) allowed the delineation of the bedrock surface below the valley floor of the Leventina in the vicinity of Chironico. Of the 40 drill cores available, 15 reached the crystalline bedrock of the Valle Leventina and 25 encountered the landslide mass but did not hit bedrock. The landslide deposits extend over a distance of 5.5 km and reach a minimum thickness up to 50–60 m. However, it is not certain if this represents the total thickness of the accumulated material, as most cores did not penetrate the base of the landslide. In drill core 36 (Fig. 8)

approximately 15 m of landslide debris is encountered, which is however not in relation with the Chironico landslide as this is too far down valley. It represents a smaller mass movement with a detachment scarp visible on the DEM on the eastern valley flank just next to the core (Fig. 7). Based on analysis of these cores, the crystalline bedrock is found at an elevation of 230 m a.s.l. downstream of the landslide and is covered by 120 m of alluvial fill of alternating gravel and sand (e.g. core 38; Fig. 8). Towards the northwest of the landslide deposit, bedrock is found at an elevation of 600 m a.s.l. This reveals a morphological step in the gneissic bedrock from northwest towards southeast. Northwest of the landslide debris, lacustrine sediments with varves were encountered. In some cores (cores 9 and 13 in Fig. 8), it is seen that lake sediments were deposited directly on top of the landslide mass, while in others they show direct contact with the bedrock (cores 8 and 10 in Fig. 8); with a thickness of 20–30 m, their distribution stretches over a length of 2.5 km. In most cores encountering lake sediments, these were overlain by a thin layer (approximately 10 m) of alluvial deposits from the Ticino river.

These subsurface observations were then used to reconstruct the pre-failure valley form (Fig. 9a). The topography of the valley bottom was estimated based on the stepped bedrock topography, suggested by the cores. Subtracting the pre-failure valley bottom model from the current valley topography (Fig. 9b), a volume of approximately 450 million m^3 was obtained for the Chironico landslide. There is evidence from field studies (Figs. 2, 4) that the Ticino and Ticinetto rivers have eroded a significant amount of material of the landslide since deposition. It was possible to calculate this eroded volume by recreating the original topography of the accumulated landslide mass directly after the release. This reconstruction is based on the shape of the remaining slide debris and the fact that a depression proximal to the release area has been observed at numerous Alpine slides (Heim 1932; Abele 1974). In other words, there is no evidence that the landslide filled the entire valley but was instead a mass predominantly on the western side. Note that the elevation of the top of the lake sediments is at 626 m (Antognini and Volpers 2002). This is an indicator of the landslide dam height, which is much lower than the maximum height of the deposit. An erosion volume of approximately 80 million m^3 was thus obtained, resulting in a total volume of 530 million m^3 for the deposit of the Chironico landslide.
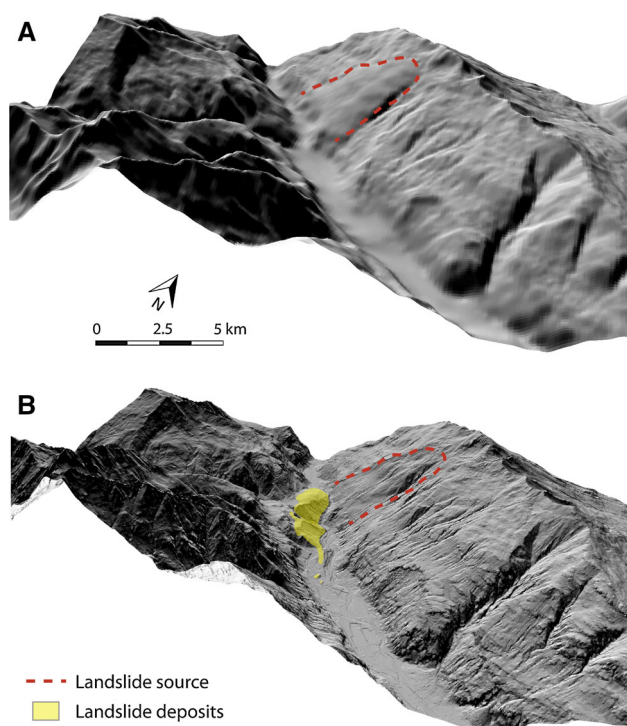

Fig. 9 DEM hillshade views of Valle Leventina at Chironico, looking towards NNW. **a** Model of the pre-failure valley based on borehole- and LiDAR interpretation. **b** Present-day valley topography with the landslide deposit

The next step is to reconstruct the topography of the pre-failure release area (outlined in red in Fig. 9a). During movement of the landslide, fragmentation and comminution of rock (Davies et al. 1999), as well as the entrainment of material, increases the volume of the deposit compared to the original volume of intact rock (e.g. Hungr 1981; Hungr and Evans 2004). Therefore, the volume of material in the release area needs to be adjusted. Typical values for bulking vary between 25 and 30 % (e.g. Hungr and Evans 2004; Pirulli 2009; Stock and Uhrhammer 2010). The volume in the release area was therefore adapted in different steps to match the volume in the accumulation area, accounting for an approximate bulking factor of 30 %. Whether this volume expansion resulted only from fragmentation of rock, or whether also some entrainment of material occurred, is not differentiated. We saw no evidence for entrained material in the field. An initial volume of intact rock on the eastern valley wall of 370 million m^3 resulted from reducing the volume of the Chironico landslide deposit by 30 %, and yielded a natural looking release area.

4.2 Runout modelling

The results of the DAN3D modelling are shown in Fig. 10. Note that a bulking factor is not taken into account by the runout model (Sosio et al. 2011) so the input volume is the same as the output volume, 530 million m^3. Evaluating the different rheologies, the run using a frictional rheology reproduced results that best matched with the observed distribution of the Chironico landslide. We applied optimized values for the basal- and internal-friction angles of 17° and 35°, respectively, found through trial and error. To obtain the maximum duration of the event, the mass was released and the velocity was observed. The time at which the landslide particles did not move anymore was then registered and the simulation time could thus be limited. From this we suggest that the Chironico landslide needed approximately 2 min to move down and fully extend into the valley. Different runs were realized with DAN3D (McDougall and Hungr 2004) and the best fitting output was plotted for a better illustration (Fig. 10). For this optimized run, the landslide achieved a maximum velocity of 110 m s^{-1}, and a runout distance of 5,160 m could be derived from the map (Fig. 10). When comparing the limits of the DAN3D output with the present landslide deposit (cross sections in Fig. 8), one has to be aware that the modelling illustrates the shape directly after the landslide has been released and it does not take into account the eroded material by the rivers. Both modelling shapes show that the landslide did not fill the entire valley as the limits are convex towards the eastern valley flank. For the northern lobe, a maximal thickness of 250 m is predicted
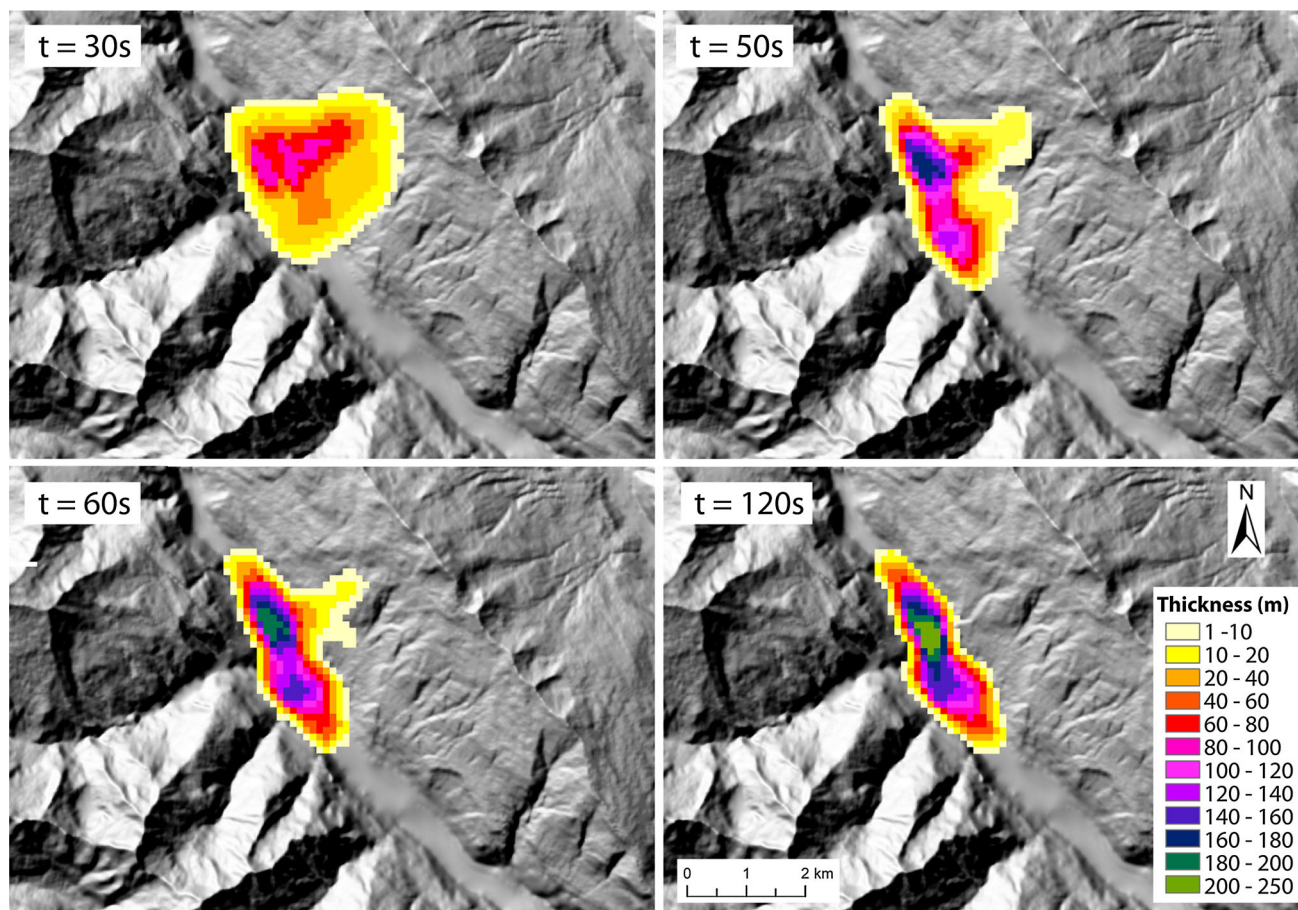
Fig. 10 Results of landslide runout modelling using the DAN3D code (McDougall and Hungr 2004). The moving mass is shown at four different time steps: after 30, 50, 60 s and finally after 120 s. The *different colours* show *the thickness* in meters of the moving mass

for the deposit, which corresponds well with the actual size of the landslide. For the southern lobe however, the thickness of the modelled landslide is, with only 160–180 m, underestimated. Furthermore, the model confirmed the location of the release area of the landslide as used as input in the model. As shown in Fig. 2, the probable release area is located on the eastern flank with a maximum elevation of ~1,775 m, comprising the region near the village of Anzonico (Fig. 1).

4.3 Surface exposure dating

AMS measured concentrations of ^{10}Be and ^{36}Cl and calculated surface exposure ages for each sample are summarized in Tables 1 and 2. Major element concentrations for sample Chi-2b are given in Table 3. The ten exposure ages for the Chironico landslide vary from 10.73 ± 0.79 to 15.46 ± 1.06 ka. The ^{36}Cl age of boulder Chi-2b, 13.20 ± 1.52 ka, is in excellent agreement with the ^{10}Be dates of both lobes (Fig. 11). Samples Chi-10 and Chi-11 are considered outliers (Fig. 11) and are thus not included in the mean calculation below. Re-evaluation of the site of Chi-10

suggests that the young age of this boulder could be explained by toppling after the deposition. The anomalously old age of sample Chi-11 might be due to an inherited concentration of cosmogenic ^{10}Be accumulated prior to failure. The age distributions including the one-standard deviation uncertainty are shown in Fig. 11. Samples Chi-5a-2, Chi-6, Chi-7 and Chi-12 originate from the northern depositional lobe (Fig. 11) and yield a mean of 13.19 ± 0.89 ka, while samples Chi-1, Chi-2b, Chi-3, Chi-4, Chi-10, Chi-11 belong to the southern lobe of the landslide accumulation area (Fig. 12) and have a mean age of 13.57 ± 1.13 ka. The errors of the mean include the uncertainty of each age and are unweighted. These results show that the ages from both lobes of the landslide deposit correlate well within the given errors. The overall mean age of the landslide is 13.41 ± 0.94 ka using only the ^{10}Be ages, and 13.38 ± 1.03 ka including both the ^{10}Be and ^{36}Cl ages.

4.4 Radiocarbon ages

Three ^{14}C dates were reported by Antognini and Volpers (2002). The dated wood fragments originated from lake

Table 2 AMS measured concentration of ^{36}Cl and calculated surface exposure age

Sample name	Latitude (DD.DD)	Longitude (DD.DD)	Elevation (m)	Boulder height (m)	Sample Thickness (cm)	Shielding correction factor	^{36}Cl (at/g) $\times 10^3$	Cl in rock (ppm)	Exposure age (ka)	Erosion corrected age using 1 mm ka^{-1} (ka)
Chi-2b	46.4139	8.8543	742	4.0	1.0	0.9818	181.40 ± 19.80	24.41 ± 0.34	13.20 ± 1.52	13.20 ± 1.52

Table 3 Major and minor element concentrations for sample Chi-2b

Elements	
SiO_2 (wt%)	70.40
Al_2O_3 (wt%)	13.70
Fe_2O_3 (wt%)	2.63
MnO (wt%)	0.05
MgO (wt%)	0.54
CaO (wt%)	1.27
Na_2O (wt%)	3.40
K_2O (wt%)	4.35
TiO_2 (wt%)	0.26
P_2O_5 (wt%)	0.10
Total	96.7
U (ppm)	3.5
Th (ppm)	12.0
B (ppm)	n.d.
Gd (ppm)	4.0
Sm (ppm)	4.5

sediments north of the landslide deposit. The wood was found at a depth of about 40 m in the core; about 6 m above the base of the lake deposits that overly blocky talus deposits. MCSN 3 was located 50 cm above MCSN 1 and 2 (Antognini and Volpers 2002). The individual obtained ages (MCSN 1: 11,340 ± 80 ^{14}C years BP, MCSN 2: 11,690 ± 85 ^{14}C years BP and MCSN 3: 11,500 ± 80 ^{14}C years BP) were converted to calendar ages with Int-Cal09 (Reimer et al. 2009) using the OxCal program (version 4.1) and applying a depositional model (Bronk Ramsey 2008). Samples MCSN1 and 2 were combined as they originated from the same depth. The recalibration resulted in a calendar age range of 13,604–13,284 cal years BP for sample MSCN 3, and 13,441–13,215 cal years BP for samples MCSN 1 and 2, and with a confidence interval of 95.4 %. Note that, according to these results, the younger age is found deeper in the core.

4.5 Local ^{10}Be production rate

Using the radiocarbon dates we can calculate a ^{10}Be production rate. We use the age from samples MCSN1 and 2, which are located deepest in the core (13,441–13,215 cal years BP), yielding a mean age of 13,328 ± 113 a. We calculated a ^{10}Be production rate based on the Chrionico data using the CRONUS-Earth online calculator (Balco et al. 2008). A sea level high latitude production rate of 3.83 ± 0.24 ^{10}Be atoms g^{-1} a^{-1} resulted for the Lm scaling scheme for spallation. The production rate is constant over time but varies according to changes in the magnetic field (Balco et al. 2008 and references therein). This production rate correlates well with that from the NE North America developmental version using the time-dependent model of Lal (1991) and Stone (2000), where $PR_{SP} = 3.88 \pm 0.19$ ^{10}Be atoms g^{-1} a^{-1} (Balco et al. 2009). Similar production rates have been obtained by Briner et al. (2012), Young et al. (2013) and Heyman (2014). Fenton et al. (2011) and Goehring et al. (2012) determined ^{10}Be production rates of rock avalanches with independent radiocarbon ages, yielding similar results.

5 Discussion

5.1 Valle Leventina evolution

During the LGM, the area around Chironico was entirely under ice except for some nunataks on the eastern and western peaks of the valley (Bini et al. 2009). With retreat of the glaciers from the Valle Leventina, steep flanks were exposed having a foliation dipping towards SSW, creating a dip-slope on the eastern flank (Antognini and Volpers 2002). After the Gschnitz stadial, around 16–17 ka (Ivy-Ochs et al. 2006), no further indication of ice occupation in the Valle Leventina is reported (Renner 1982; Hantke 1983). Therefore the glaciers deposited all glacial and glaciofluvial sediments mapped today on both valley flanks during the LGM or early Lateglacial. After glacier withdrawal, the Ticinetto occupied a course probably flowing straight from Chironico into the Ticino. This statement is based on the fact that during the construction of a tunnel alluvial sediments of the Ticinetto were encountered, underlying the landslide debris below the village of Chironico (Schardt 1910). Thus, the confluence of both rivers was situated a few 100 m upstream of today's confluence.

Fig. 11 Plot of the surface exposure ages and calibrated radiocarbon dates of the Chironico landslide, inserted schematically on a northwest-southeast profile (cf. Fig. 8). The *grey line* shows the mean age of the landslide with 13.38 ± 1.03 ka (the error is illustrated by the *grey band*). The main valley was ice-free by at least 17 ka BP (before the Gschnitz stadial (*blue band*); Renner 1982, Hantke 1983)
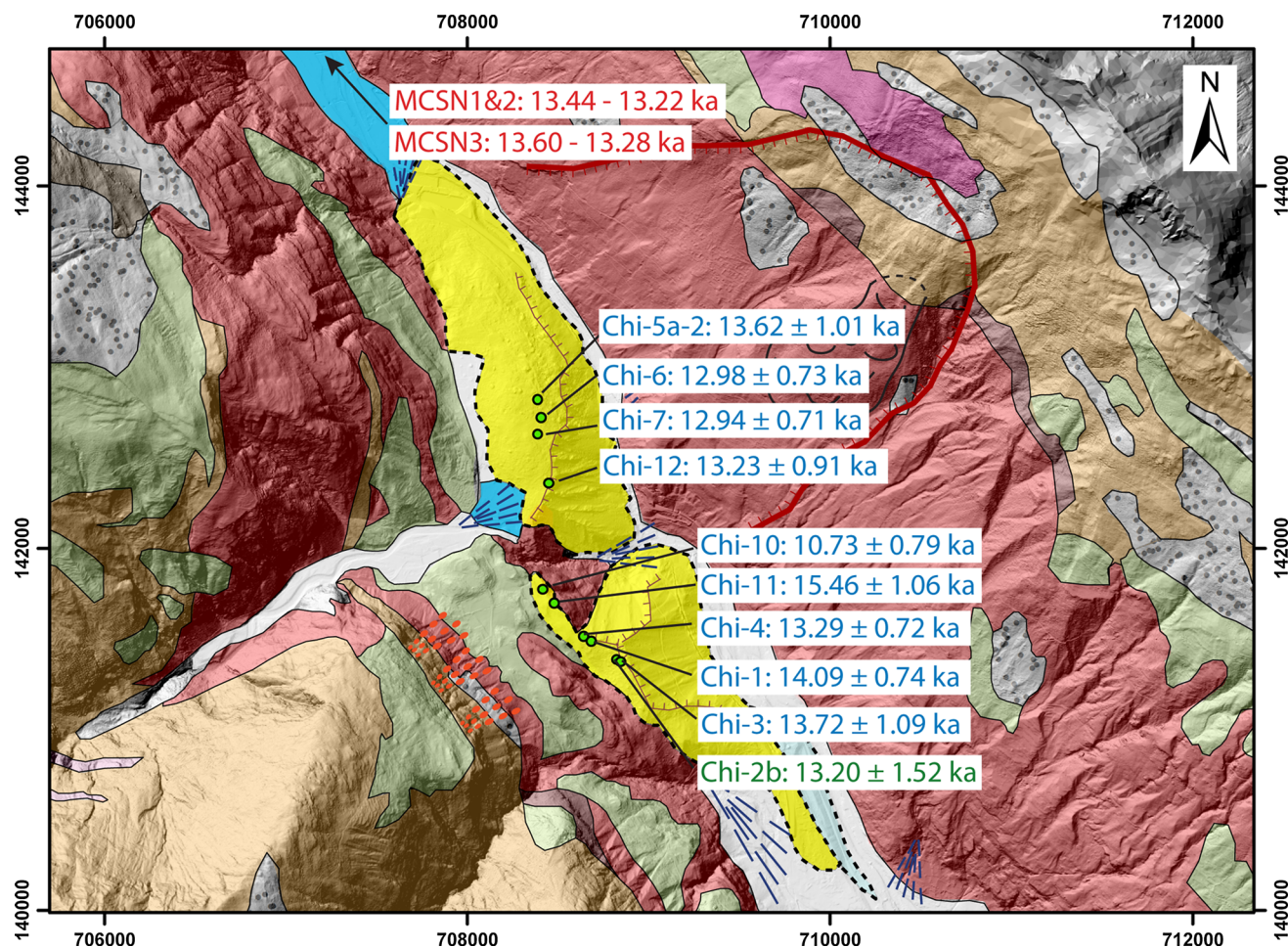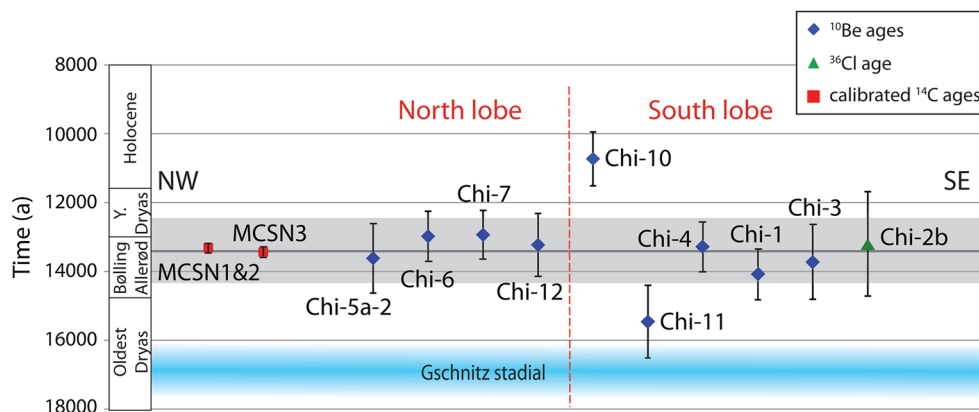

Fig. 12 Summary of all the ages obtained from the landslide deposits by Chironico, Valle Leventina, superimposed on the geological-geomorphological map (Fig. 3)

The calculated exposure ages (Fig. 11) are consistent with an average age of 13.38 ± 1.03 ka. The Chironico landslide is thus the only landslide absolutely dated to the Lateglacial period, with the exception of the Almtal landslide, which has an age of 15.60 ± 1.10 ka BP (van Husen et al. 2007). Most known large prehistoric landslides failed during the Holocene (e.g. Poschinger 2002; Soldati et al. 2004; Gruner 2006; Prager et al. 2008; Ivy-Ochs et al. 1998, 2009). Furthermore, the exposure ages, even taking into account measurement errors, demonstrate that the

northern and southern lobes belong to one single landslide, implying that the Chironico landslide was a single event which occurred during the Bølling-Allerød interstadial between 14,700 and 12,900 BP. This result contradicts the earlier interpretation by Naegeli (1920) and Dal Vesco (1979) that the deposits of the Chironico landslide are the outcome of two different events, and confirms the interpretation of Antognini and Volpers (2002) that this landslide was one event.

The landslide then dammed the Ticino River, and a lake with a length of 3 km (Antognini and Volpers 2002) formed northwest of the debris accumulation. This then filled up with lacustrine sediments having a thickness of about 20–30 m. An estimated duration for the lake is between 120 and 730 years based on sediment yield estimations for the late Pleistocene (Antognini and Volpers 2002 and references therein). The Ticino filled the lake and then subsequently incised its course into the northern and southern depositional lobes (Fig. 3). Besides the Ticino river, the Ticinetto was also blocked by the sliding mass, building a lake near the village of Chironico (Fig. 3) at an elevation of approximately 750 m. The discharge of this second lake might have been over the top of the plain of Chironico, where depressions can be observed today. During this time, the confluence of Ticinetto and Ticino was situated near Lavorgo (Schardt 1910; Fig. 1), which would explain the alluvial fan towards the northern end of the landslide deposit. After the lake was filled with sediments, and alluvium accumulated towards the north of the Chironico plain, the Ticinetto finally breached the landslide deposit along its present course (Fig. 3). The large amount of incision here suggests this occurred soon after landslide deposition, as a significant amount of material is missing today (Fig. 2). A third river that was influenced by the landslide was the Baroglia. It was diverted by the southern lobe (Antognini and Volpers 2002) to such an extent that it flows today into the Ticino further downstream than in the past. A large alluvial fan comprised of mobilized landslide debris was created to the west of the southernmost end of the landslide deposit (Fig. 3). The curved western margin of the southern landslide mass was thus created by the river. It took some time after release of the landslide for the fluvial environment to stabilize as towards the southwest, the Baroglia river re-incised into its own alluvial deposits after aggradation ceased. On the eastern side of the southern lobe, a wide and flat braided-stream area is observed on the valley bottom. Today, incision ends at this point as evidenced by the alluviation of the plain.

Post-failure movements also affected the landslide detachment area and a minor rock slope failure is observed in the release area (Fig. 3), which is also younger than the landslide.

5.2 Runout modelling

The runout distance and lateral expansion of the landslide deposit was replicated in a numerical model (DAN3D; McDougall and Hungr 2004). The fact that the landslide was deposited into the Ticinetto stream on the western flank, blocking the stream, could also be reproduced. Though the sliding mass seemed to split into two different lobes after 50 s (Fig. 9), the final shape does not show such an obvious distribution. This may be related to the bedrock step in the release area (E–W trending, north facing scarp, Fig. 2) and it may, to some extent, also be controlled by the bedrock step along the bed of the Ticino river.

Although the modelling revealed good results, there are some limiting boundary conditions. The morphology of the release area and the sliding surface have a strong influence on both the volume of the landslide deposit, as well as on the spreading and ultimate extent of the moving mass (Sosio et al. 2008). Potential effects on the runout model originated from estimation of the position of the detachment scarp, as there is no clear evidence of its location in the field nor can it be clearly identified on the LiDAR image. The following reasons however, suggest a location on the eastern valley flank near the village of Anzonico, as outlined on the map in Fig. 3. Firstly, the proximal depression on the western valley wall above the deposit area, as well as the shape of the landslide deposit with the bulge against this flank, indicate that the landslide must have been released from the eastern flank of the Valle Leventina. Secondly, the lithology of the landslide deposit consists mainly of Leventina orthogneiss (Lautensach 1912; Antognini and Volpers 2002). On the western valley wall, orthogneiss is only present at lower elevations, whereas on the eastern wall, Leventina gneiss can be found at elevations of up to 1,400 m (the topmost release area is situated at ∼1,775 m). Thirdly, the presence of numerous post-LGM glacial and glaciofluvial deposits, apparently older than the landslide, on the western valley side (Fig. 3) indicates that the slide cannot have been released from this flank of the Valle Leventina. This is supported by the absence of glacial sediments on the eastern valley flank in the detachment area, suggesting that till from this side was probably moved together with the sliding mass (Abele 1974; Poschinger 2002; Prager et al. 2008).

Our detailed landscape analysis established a depositional volume of 530 million m^3 for the landslide, which fits well with previous volume estimations of 300–500 million m^3 (Abele 1974), 600 million m^3 (Schardt 1910) and 500–600 million m^3 (Naegeli 1920). This implies that the Chironico landslide is one of the largest landslides in the Alps in crystalline rock, alongside the Köfels landslide with a volume >3.2 km^3 (Abele 1974; Heuberger 1994; Brückl et al. 2001), and the Totalp landslide, with a

released volume of approximately 600 million m³ (Abele 1974; Maisch 1981).

5.3 Preparatory and triggering mechanisms

It is difficult to evaluate which failure mechanisms were involved in the release of the Chironico landslide as often several processes that decrease rock strength interact with each other (Prager et al. 2008 and references therein). A predisposed factor, which makes the eastern wall of the Valle Leventina susceptible to mass movements, is the dip-slope. The results of our surface exposure dating indicate clearly post-glacial ages and therefore an immediate deglaciation-related failure can be ruled out; the release of the landslide was delayed by a few thousand years compared to deglaciation (Fig. 11). This result is consistent with recent data of Ballantyne et al. (2013, 2014a, b), who observed enhanced rock-slope failure in Ireland and Scotland approximately 2,000 years after deglaciation. Thus, a preparatory factor, which cumulated over a long period of time, is stress redistribution during glacial unloading (Heim 1932; Prager et al. 2007, 2008), which might have also initiated internal slope fracturing (Ballantyne et al. 2014a, b). A direct triggering factor however, would be a heavy rainfall episode or an earthquake (Gunzburger et al. 2005). It is known from the literature that many historic landslides are triggered by heavy rainfall (Eisbacher and Clague 1984; Gruner 2006). Although there exist no records on rainfall during these times, this triggering factor cannot be excluded. Evaluating the role of seismic activity as a regional triggering factor in the case of the Chironico landslide is more complex as there is no record of a strong earthquake in the Chironico area at that time. In the palaeoseismic event catalogue of Central Switzerland (Monecke et al. 2006; Strasser et al. 2013) however, some events are registered in the northern part of the Alps during the Lateglacial, namely in the sediments of Lake Lucerne and Lake Zurich. In the Southern Alps, large turbidite deposits that might be related to strong earthquakes were recorded in Lake Iseo (Lauterbach et al. 2012) and Lake Como (Fanetti et al. 2008) during the Holocene. This might be a hint that large seismic events similar to those in the northern part of the Central Alps also occurred in the southern part during the Lateglacial.

6 Conclusions

The Chironico landslide in the southern Swiss Alps, consisting of two lobes with a total volume of 530 million m³, is one of the largest landslides in the Alps in crystalline rock. Absolute age determination of the landslide using the cosmogenic nuclides ¹⁰Be and ³⁶Cl on ten boulders yielded

a mean age of 13.38 ± 1.03 ka with excellent agreement between ¹⁰Be and ³⁶Cl ages. This landslide is the oldest in the Alps in crystalline rock.

Geological and geomorphological investigation of the study area enabled us to understand the landscape evolution history of the Valle Leventina around Chironico. The landslide blocked both the Ticino and Ticinetto rivers and consequently two lakes were formed. From the subsurface observations it is noticeable that the Ticino river prograded over the lake and incised its course into both depositional lobes. At that time, the confluence of the Ticinetto and the Ticino rivers was situated near Lavorgo. Only after the second lake was filled with sediments, and alluvium accumulated towards the north of the Chironico plain, did the Ticinetto finally breach the landslide deposit along its present course.

The time lag between deglaciation and landslide failure suggests that the landslide might have been related to glacial unloading, though with a few thousand years of delay. Glacier withdrawal prepared the failure by exposing steep flanks with a dip-slope on the eastern side of the Valle Leventina.

The character and extent of motion of the Chironico landslide was reproduced using DAN3D runout modelling (McDougall and Hungr 2004) confirming a single event scenario. Furthermore, our modelling suggests that the detachment scarp was located on the eastern Valle Leventina flank at an elevation of up to ~1,775 m.

Due to the fact that the exposure ages revealed good agreement with available radiocarbon dates from the wood fragments, the results could be used for calibration of the ¹⁰Be production rate of the study area. A local sea level high latitude reference production rate of 3.83 ± 0.24 atoms $g^{-1} a^{-1}$ resulted for the Lm scaling scheme for spallation.

References

Abele, G. (1974). *Bergstürze in den Alpen, ihre Verbreitung, Morphologie und Folgeerscheinungen* (230 pp). Wissenschaftliche Alpenvereinshefte, 25, München.

Akçar, N., Deline, P., Ivy-Ochs, S., Alfimov, V., Hajdas, I., Kubik, P. W., et al. (2012). The AD 1717 rock avalanche deposits in the

upper Ferret Valley (Italy): A dating approach with cosmogenic [10]Be. *Journal of Quaternary Science, 27*(4), 383–392.

Alfimov, V., & Ivy-Ochs, S. (2009). How well do we understand the production of [36]Cl in limestone and dolomite? *Quaternary Geochronology, 4,* 462–474.

Ambrosi, C., & Crosta, G. B. (2011). Valley shape influence on deformation mechanisms of rock slopes. *Geological Society London Special Publications, 351,* 215–233.

Antognini, M., & Volpers, R. (2002). A late Pleistocene age for the Chironico rockslide (Central Alps, Ticino, Switzerland). *Bulletin for Applied Geology, 7*(2), 113–125.

Balco, G., Briner, J., Finkel, R. C., Rayburn, J. A., Ridge, J. C., & Schaefer, J. M. (2009). Regional beryllium-10 production rate calibration for northeastern North America. *Quaternary Geochronology, 4,* 93–107.

Balco, G., Stone, J. O., Lifton, N. A., & Dunai, T. J. (2008). A complete and easily accessible means of calculating surface exposure ages or erosion rates from Be-10 and Al-26 measurements. *Quaternary Geochronology, 3,* 174–195.

Ballantyne, C. K., Sandeman, G. F., Stone, J. O., & Wilson, P. (2014a). Rock-slope failure following Late Pleistocene deglaciation on tectonically stable mountainous terrain. *Quaternary Science Reviews, 86,* 144–157.

Ballantyne, C. K., Wilson, P., Gheorghiu, D., & Rodes, A. (2014b). Enhanced rock-slope failure following ice-sheet deglaciation: Timing and causes. *Earth Surface Processes and Landforms, 39,* 900–913.

Ballantyne, C. K., Wilson, P., Schnabel, C., & Xu, S. (2013). Lateglacial rock slope failures in north-west Ireland: Age, causes and implications. *Journal of Quaternary Science, 28*(8), 789–802.

Bini, A., Buoncristiani, J. -F., Couterrand, S., Ellwanger, D., Felber, M., Florineth, D., Graf, H. R., Keller, O., Kelly, M., Schlüchter, C., Schoeneich, P. (2009). *Die Schweiz während des letzteiszeitlichen Maximums (LGM), 1:500 000.* Federal Office of Topography, swisstopo. Wabern, Switzerland.

Borgatti, L., & Soldati, M. (2010). Landslides as a geomorphological proxy for climate change: A record from the Dolomites (northern Italy). *Geomorphology, 120,* 56–63.

Briner, J. P., Young, N. E., Goehring, B. M., & Schaefer, J. M. (2012). Constraining Holocene [10]Be production rates in Greenland. *Journal of Quaternary Science, 27*(1), 2–6.

Bronk Ramsey, C. (2008). Deposition models for chronological records. *Quaternary Science Reviews, 27*(1–2), 42–60.

Brückl, E., Brückl, J., & Heuberger, H. (2001). Present structure and prefailure topography of the giant rockslide Köfels. *Zeitschrift für Gletscherkunde und Glazialgeologie, 37,* 49–79.

Casasopra, S. (1939). Studio petrografico dello Gneiss granitico Leventina (Valle Riviera e Valle Leventina, Canton Ticino). *Schweizerische Mineralogische und Petrographische Mitteilungen, 19,* 449–709.

Chmeleff, J., von Blanckenburg, F., Kossert, K., & Jakob, D. (2010). Determination of the [10]Be half-life by multicollector ICP-MS and liquid scintillation counting. *Nuclear Instruments and Methods in Physics Research Section B Beam Interactions with Materials and Atoms, 268*(2), 192–199.

Dal Vesco, E. (1979). Viadotto della Biaschina: Geologie des Baugrundes. *Schweizerischer Ingenieur und Architektenverein, 97*(38), 739–741.

Dapples, F., Oswald, D., Raetzo, H., Lardelli, T., & Zwahlen, P. (2003). New records of Holocene landslide activity in the Western and Eastern Swiss Alps: Implication of climate and vegetation changes. *Eclogae Geologicae Helvetiae, 96,* 1–9.

Davies, T. R., McSaveney, M. J., & Hodgson, K. A. (1999). A fragmentation-spreading model for long-runout rock avalanches. *Canadian Geotechnical Journal, 36*(6), 1096–1110.

Desilets, D., Zreda, M., Almasi, P. F., & Elmore, D. (2006). Determination of cosmogenic [36]Cl in rocks by isotope dilution: innovations, validation and error propagation. *Chemical Geology, 233,* 185–195.

Eisbacher, G. & Clague, J. J. (1984). Destructive mass movements in high mountains: Hazard and management, *Geological Survey of Canada,* Paper 84–16.

Evans, J., Stone, J., Fifield, L., & Cresswell, R. (1997). Cosmogenic chlorine-36 production in K-feldspar. *Nuclear Instruments and Methods in Physics Research Section B Beam Interactions with Materials and Atoms, 123,* 334–340.

Fanetti, D., Anselmetti, F. S., Chapron, E., Sturm, M., & Vezzoli, L. (2008). Megaturbidites deposits in the Holocene basin fill of Lake Como (Southern Alps, Italy). *Palaeogeography Palaeoclimatology Palaeoecology, 259,* 323–340.

Fenton, C. R., Hermanns, R. L., Blikra, L. H., Kubik, P. W., Bryant, C., Niedermann, S., et al. (2011). Regional 10Be production rate calibration for the past 12 ka deduced from the radiocarbondated Grøtlandsura and Russenes rock avalanches at 69N, Norway. *Quaternary Geochronology, 6,* 437–452.

Fritsche, S., & Fäh, D. (2009). The 1946 magnitude 6.1 earthquake in the Valais: Site-effects as contributor to the damage. *Eclogae Geologicae Helvetiae, 102,* 423–439.

Goehring, B. M., Lohne, O. S., Mangerud, J., Svendsen, J. I., Gyllencreutz, R., Schaefer, J., et al. (2012). Late Glacial and Holocene [10]Be production rates for western Norway. *Journal of Quaternary Science, 27*(1), 89–96.

Gosse, J., & Philips, F. (2001). Terrestrial in situ cosmogenic nuclides: Theory and application. *Quaternary Science Reviews, 20,* 1475–1560.

Gross, G., Kerschner, H., & Patzelt, G. (1978). Methodische Untersuchungen über die Schneegrenze in den alpinen Gletschergebieten. *Zeitschrift für Gletscherkunde und Glaziogeologie, 12,* 223–251.

Gruber, A., Strauhal, T., Prager, C., Reitner, J., Brandner, R., & Zangerl, C. (2009). Die Butterbichl-Gleitmasse – eine grosse fossile Massenbewegung am Südrand der Nördlichen Kalkalpen (Tirol, Österreich). *Bulletin für angewandte Geologie, 14,* 103–134.

Gruner, U. (2006). Bergstürze und Klima in den Alpen – gibt es Zusammenhänge? *Bulletin für angewandte Geologie, 11*(2), 25–34.

Gunzburger, Y., Merrien-Soukatchoff, V., & Guglielmi, Y. (2005). Influence of daily surface temperature fluctuations on rock slope stability: Case study of the Rocher de Valabres slope (France). *International Journal of Rock Mechanics and Mining Sciences, 42,* 331–349.

Hantke, R. (1983). *Eiszeitalter. Die jüngste Erdgeschichte der Schweiz und ihrer Nachbargebiete. Band 3: Westliche Ostalpen mit ihrem bayerischen Vorland bis zum Inn-Durchbruch und Südalpen zwischen Dolomiten und Mont Blanc* (730 pp). Thun: Ott Verlag.

Heim, A. (1932). *Bergsturz und Menschenleben* (218 pp). Beiblatt zur Vierteljahresschrift der Natruforschenden Gesellschaft Zürich.

Heuberger, H. (1994). The giant landslide of Köfels, Ötztal, Tyrol. *Mountain Research and Development, 14*(4), 290–294.

Heyman, J. (2014). Paleoglaciation of the Tibetan Plateau and surrounding mountains based on exposure ages and ELA depression estimates. *Quaternary Science Reviews, 91,* 30–41.

Hovius, N., & Stark, C. P. (2007). Landslide-driven erosion and topographic evolution of active mountain belts. In S. G. Evans, G. Scarascia Mugnozza, A. Strom, & R. L. Hermanns (Eds.), *Landslides from massive rock slope failure 49* (pp. 573–590). Dordrecht: Springer.

Hovius, N., Stark, C. P., & Allen, P. A. (1997). Sediment flux from a mountain belt derived from landslide mapping. *Geology, 25,* 231–234.

Hungr, O. (1981). Dynamics of rock avalanches and other types of mass movements. *Ph.D. dissertation*, University of Alberta, Edmonton, Canada.

Hungr, O., & Evans, S. G. (1996). Rock avalanche runout prediction using a dynamic model. In *Proceedings, 7th International symposium on landslides, 1*, pp. 233–238.

Hungr, O., & Evans, S. G. (2004). Entrainment of debris in rock avalanches: An analysis of a long run-out mechanism. *Geological Society of America Bulletin, 116*(9–10), 1240–1252.

Hungr, O., & McDougall, S. (2009). Two numerical models for landslide dynamic analysis. *Computers and Geosciences, 35*, 978–992.

Ivy-Ochs, S. (1996). The dating of rock surfaces using in situ produced ^{10}Be, ^{26}Al and ^{36}Cl, with examples from Antarctica and the Swiss Alps. *Ph.D. dissertation*, ETH Zurich, Zurich, Switzerland.

Ivy-Ochs, S., Heuberger, H., Kubik, P.W., Kerschner, H., Bonani, G., Frank, M., Schlüchter, C. (1998). The age of the Köfels event. Relative, ^{14}C and cosmogenic isotope dating of an early Holocene landslide in the Central Alps (Tyrol, Austria). *Zeitschrift für Gletscherkunde und Glazialgeologie, 34(1)*, 57–68.

Ivy-Ochs, S., Kerschner, H., Kubik, P. W., & Schlüchter, C. (2006). Glacier response in the European Alps to Heinrich event 1 cooling: The Gschnitz stadial. *Journal of Quaternary Science, 21*, 115–130.

Ivy-Ochs, S., & Kober, F. (2008). Surface exposure dating with cosmogenic nuclides. *E&G Quaternary Science Journal, 57*(1–2), 179–209.

Ivy-Ochs, S., Poschinger, Av, Synal, H. A., & Maisch, M. (2009). Surface exposure dating of the Flims landslide, Graubünden, Switzerland. *Geomorphology, 103*, 104–112.

Ivy-Ochs, S., Synal, H.-A., Roth, C., & Schaller, M. (2004). Initial results from isotope dilution for Cl and ^{36}Cl measurements at the PSI/ETH Zürich AMS facility. *Nuclear Instruments and Methods in Physics Research Section B Beam Interactions with Materials and Atoms, 223–224*, 623–627.

Korschinek, G., Bergmaier, A., Faestermann, T., Gerstmann, U., Knie, K., Rugel, G., et al. (2010). A new value for the half-life of ^{10}Be by Heavy-Ion Elastic Recoil Detection and liquid scintillation counting. *Nuclear Instruments and Methods in Physics Research Section B Beam Interactions with Materials and Atoms, 268*, 187–191.

Korup, O., Densmore, A. L., & Schlunegger, F. (2010). The role of landslides in mountain range evolution. *Geomorphology, 120*, 77–90.

Kubik, P. W., & Christl, M. (2010). ^{10}Be and ^{26}Al measurements at the Zurich 6 MV Tandem AMS facility. *Nuclear Instruments and Methods in Physics Research Section B Beam Interactions with Materials and Atoms, 268*, 880–883.

Lal, D. (1991). Cosmic ray labeling of erosion surfaces: In situ nuclide production rates and erosion models. *Earth and Planetary Science Letters, 104*, 424–439.

Lautensach, H. (1912). *Die Übertiefung des Tessingebiets: morphologische Studie* (156 pp.). Geographische Abhandlungen der Universität Berlin, Heft 1. Leibzig: Teubner Verlag.

Lauterbach, S., Chapron, E., Brauer, A., Hüls, M., Gilli, A., Arnaud, F., et al. (2012). A sedimentary record of Holocene surface runoff events and earthquake activity from Lake Iseo (Southern Alps, Italy). *The Holocene, 22*(7), 749–760.

Liu, B., Phillips, F. M., Fabryka-Martin, J. T., Fowler, M. M., & Stone, W. D. (1994). Cosmogenic ^{36}Cl accumulation in unstable landforms, 1. Effects of the thermal neutron distribution. *Water Resources Research, 30*, 3115–3125.

Maisch, M. (1981). Glazialmorphologische und gletschergeschichtliche Untersuchungen im Gebiet zwischen Landwasser- und

Albulatal (KT. Graubünden, Schweiz): Physische Geographie, Volume 3. *Ph.D. dissertation,* Universität Zürich, Zurich, Switzerland.

McDougall, S., & Hungr, O. (2004). A model for the analysis of rapid landslide motion across three-dimensional terrain. *Canadian Geotechnical Journal, 41*, 1084–1097.

Monecke, K., Anselmetti, F. S., Becker, A., Schnellmann, M., Sturm, M., & Giardini, D. (2006). Earthquake-induced deformation structures in lake deposits: A late Pleistocene to Holocene paleoseismic record for Central Switzerland. *Eclogae Geologicae Helvetiae, 99*, 343–362.

Müller, A., Christl, M., Lachner, J., Suter, M., & Synal, H.-A. (2010). Competitive ^{10}Be measurements below 1 MeV with the upgraded ETH-TANDY AMS facility. *Nuclear Instruments and Methods in Physics Research Section B Beam Interactions with Materials and Atoms, 268*(17–18), 2801–2807.

Naegeli, H. (1920). Die postglazial-prähistorischen Biaschina-Bergstürze. *Ph.D. dissertation,* Universität Zürich, Zurich, Switzerland.

Niggli, P., Preiswerk, H., Grütter, O., Bosshard, L., Kündig, E. (1936). Geologische Beschreibung der Tessiner Alpen zwischen Maggia- und Bleniotal. *Beiträge zur Geologischen Karte der Schweiz N.F.71*, 1–190.

Nishiizumi, K., Imamura, M., Caffee, M. W., Southon, J. R., Finkel, R. C., & McAnich, J. (2007). Absolute calibration of ^{10}Be AMS standards. *Nuclear Instruments and Methods in Physics Research Section B Beam Interactions with Materials and Atoms, 258*, 403–413.

Ochs, M., & Ivy-Ochs, S. (1997). The chemical behaviour of Be, Al, Fe, Ca and Mg during AMS target preparation from terrestrial silicates modeled with chemical speciation calculations. *Nuclear Instruments and Methods in Physics Research Section B Beam Interactions with Materials and Atoms, 123*, 235–240.

Phillips, F. M., Stone, W. D., & Fabryka-Martin, J. T. (2001). An improved approach to calculating low-energy cosmic-ray neutron fluxes near the land/atmosphere interface. *Chemical Geology, 175*, 689–701.

Pirulli, M. (2009). The Thurwieser rock avalanche (Italian Alps): Description and dynamic analysis. *Engineering Geology, 109*, 80–92.

Pirulli, M., Bristeau, M. O., Mangeney, A., & Scavia, C. (2007). The effect of the earth pressure coefficients on the runout of granular material. *Environmental Modelling and Software, 22*, 1437–1454.

Poschinger, A.V. (2002). Large rockslides in the Alps: A commentary on the contribution of G. Abele (1937–1994) and a review of some recent developments. In Evans, G., De Graf, J. V. (eds), *Catastrophic landslides: Effects, occurrence and mechanisms* (pp. 237–255). Boulder: Geological Society of America Reviews in Engineering Geology, 15.

Prager, C., Ivy-Ochs, S., Ostermann, M., Synal, H. A., & Patzelt, G. (2009). Geological considerations and age of the catastrophic Fernpass rockslide (Tyrol, Austria). *Geomorphology, 103*, 93–103.

Prager, C., Zangerl, C., Brandner, R., Patzelt, G. (2007). Increased rockslide activity in the middle Holocene? New evidence from the Tyrolean Alps (Tyrol, Austria). In Mathie, E., Mc Innes, R., Jakeways, J., Fairbank, H., *Landslides and climate change: Challenges and Solutions* (pp. 25–34). London: Taylor & Francis.

Prager, C., Zangerl, C., Patzelt, G., & Brandner, R. (2008). Age distribution of fossil landslides in the Tyrol (Austria) and its surrounding areas. *Natural Hazards and Earth System Sciences, 8*, 377–407.

Preiswerk, H., Bossard, L., Grütter, O., Niggli, P., Kündig, E., & Ambühl, E. (1934). *Geologische Karte der Tessiner Alpen*

zwischen Maggia- und Bleniotal, 1:50 000. Spezialkarte Nr: Geologische Karte der Schweiz. 116.

Raetzo-Brühlhart, H. (1997). *Massenbewegungen im Gurnigelflysch und Einfluss der Klimaänderung* (256 pp.). Schlussbericht NFP 31. Zürich: vdf Hochschulverlag AG, ETH Zürich.

Reimer, P. J., Baillie, M. G. L., Bard, E., Byliss, A., Beck, J. W., Blackwell, P. G., et al. (2009). IntCal09 and Marine09 radiocarbon age calibration curves, 0–50,000 years cal BP. *Radiocarbon, 51*(4), 1111–1150.

Renner, F. B. (1982). Beiträge zur Gletschergeschichte des Gotthardgebietes und dendroklimatologische Analysen an fossilen Hölzern. *Ph.D. dissertation,* Universität Zürich, Zurich, Switzerland.

Ruetti, R., Maxelon, M., & Mancktelow, N. S. (2005). Structure and kinematics of the northern Simano Nappe, Central Alps, Switzerland. *Eclogae Geologicae Helvetiae, 9*(1), 63–81.

Schardt, H. (1910). L'éboulement préhistorique de Chironico (Tessin). *Bollettino della Società Ticinese di Scienze Naturali, 6,* 76–91.

Shroder, J. F., & Bishop, M. P. (1998). Mass movement in the Himalaya: New insights and research directions. *Geomorphology, 26,* 13–35.

Soldati, M., Corsini, A., & Pasuto, A. (2004). Landslides and climate change in the Italian Dolomites since the Late Glacial. *Catena, 55,* 141–161.

Sosio, R., Crosta, G. B., & Hungr, O. (2008). Complete dynamic modelling calibration for the Thurwieser rock avalanche (Italian Central Alps). *Engineering Geology, 100,* 11–26.

Sosio, R., Crosta, G. B., & Hungr, O. (2011). Numerical modelling of debris avalanche propagation from collapse of volcanic edifices. *Landslides, 9,* 315–334.

Stock, G. M., & Uhrhammer, R. (2010). Catastrophic rock avalanche 3600 years BP from El Capitan, Yosemite Valley, California. *Earth Surface Processes and Landforms, 35,* 941–951.

Stone, J. O. (2000). Air pressure and cosmogenic isotope production. *Journal of Geophysical Research, 105*(B10), 23753–23759.

Stone, J. O., Allan, G., Fifield, L., & Cresswell, R. (1996). Cosmogenic chlorine-36 from calcium spallation. *Geochimica et Cosmochimica Acta, 60*(4), 679–692.

Stone, J. O. H., Evans, J., Fifield, L., Allan, G., & Cresswell, R. (1998). Cosmogenic chlorine-36 production in calcite by muons. *Geochimica et Cosmochimica Acta, 62*(3), 433–454.

Strasser, M., Monecke, K., Schnellmann, M., & Anselmetti, F. S. (2013). Lake sediments as natural seismographs: A compiled record of Late Quaternary earthquakes in Central Switzerland and its implication for Alpine deformation. *Sedimentology, 60,* 319–341.

Synal, H.-A., Bonani, G., Döbeli, M., Ender, R., Gartenmann, P., Kubik, P., et al. (1997). Status report of the PSI/ETH AMS facility. *Nuclear Instruments and Methods in Physics Research Section B Beam Interactions with Materials and Atoms, 123,* 62–68.

Timar-Geng, Z., Grujic, D., & Rahn, M. (2004). Deformation at the Leventina-Simano nappe boundary, Central Alps, Switzerland. *Eclogae Geologicae Helvetiae, 97,* 265–278.

van Husen, D., Ivy-Ochs, S., & Alfimov, V. (2007). Mechanism and age of Late Glacial landslides in the Calcareous Alps; the Almtal landslide, Upper Austria. *Austrian Journal of Earth Sciences, 100,* 114–126.

von Blanckenburg, F., Belshaw, N. S., & O'Nions, R. K. (1996). Separation of ^{9}Be and cosmogenic ^{10}Be from environmental materials and SIMS isotope dilution analysis. *Chemical Geology, 129*(1–2), 93–99.

Young, N. E., Schaefer, J. M., Briner, J. P., & Goehring, B. M. (2013). A ^{10}Be production-rate calibration for the Arctic. *Journal of Quaternary Science, 28*(5), 515–526.